CORE
Metadata, citation and similar papers at core.ac.uk
Provided by Digital.CSIC

AIP | Journal of Applied Physics

Monte Carlo simulation of damage and amorphization induced by swift-ion irradiation in LiNbO3

G. García, F. Agulló-López, J. Olivares-Villegas, and A. García-Navarro

Citation: J. Appl. Phys. **99**, 053504 (2006); doi: 10.1063/1.2175464
View online: http://dx.doi.org/10.1063/1.2175464
View Table of Contents: http://jap.aip.org/resource/1/JAPIAU/v99/i5
Published by the American Institute of Physics.

Additional information on J. Appl. Phys.

Journal Homepage: http://jap.aip.org/
Journal Information: http://jap.aip.org/about/about_the_journal
Top downloads: http://jap.aip.org/features/most_downloaded
Information for Authors: http://jap.aip.org/authors

ADVERTISEMENT

Downloaded 23 Jan 2013 to 161.111.22.141. Redistribution subject to AIP license or copyright; see http://jap.aip.org/about/rights_and_permissions

Monte Carlo simulation of damage and amorphization induced by swift-ion irradiation in $LiNbO_3$

G. García[a)]
Centro de Micro-Análisis de Materiales, Universidad Autónoma de Madrid, C/Faraday 3, Campus de Cantoblanco, 28049 Madrid, Spain

F. Agulló-López
Centro de Micro-Análisis de Materiales, Universidad Autónoma de Madrid, C/Faraday 3, Campus de Cantoblanco, 28049 Madrid, Spain and Departamento de Física de Materiales, Universidad Autónoma de Madrid, C/Faraday 3, Campus de Cantoblanco, 28049 Madrid, Spain

J. Olivares-Villegas
Centro de Micro-Análisis de Materiales, Universidad Autónoma de Madrid, C/Faraday 3, Campus de Cantoblanco, 28049 Madrid, Spain and Instituto de Óptica "Daza de Valdés"-CSIC, Madrid, C/Serrano 121, 28006 Madrid, Spain

A. García-Navarro
Centro de Micro-Análisis de Materiales, Universidad Autónoma de Madrid, C/Faraday 3, Campus de Cantoblanco, 28049 Madrid, Spain

(Received 8 August 2005; accepted 24 January 2006; published online 2 March 2006)

This paper presents a Monte Carlo (MC) simulation tool which is applied to describe the ion beam induced damage generated by electronic excitation in $LiNbO_3$. Based on a previously published thermal spike based analytical model, the MC technique allows for a more flexible and accurate treatment of the problem. A main advantage of this approach with respect to the analytical one is the possibility of studying the role of statistical fluctuations, relevant at low fluences. The paper recalls the main features of the physical model, describes the MC algorithm, and compares simulation results to experimental data (irradiations of $LiNbO_3$ using silicon ions at 5 and 7.5 MeV and oxygen ions at 5 MeV). © *2006 American Institute of Physics*. [DOI: 10.1063/1.2175464]

I. INTRODUCTION

It is well known that the ion irradiation of a crystal produces permanent damage via nuclear (collisional) energy loss. This mechanism becomes more effective for low energies occurring at the end of the range where ions are implanted.[1–4] At high fluences, the damage leads to lattice amorphization, that has been used for the fabrication of optical waveguides and integrated optics devices.[4] In the high energy regime, electronic energy loss can also produce damage and even amorphization provided that the local energy density deposited by the incoming ion (i.e., the electronic stopping power) is above a given threshold level, which is material dependent. Under these conditions each bombarding ion generates a latent (amorphous) track of nanometric diameter along its trajectory.[5–7] At fluences where single tracks overlap a homogeneous heavily damaged and/or amorphous layer is produced that has been experimentally observed and investigated.[8–12] There are several theoretical approaches to describe the electronic excitation damage and amorphization. So far, thermal spike models have provided a simple and useful explanation for the damage process and particularly the thresholding effect for amorphization.[13–15] Moreover, gross features and main trends are reasonably described. Other approaches, e.g., molecular dynamics models,[16,17] although presenting a more advanced and rigorous analysis, are much more complicated to implement and have been less used. Recently, the thermal spike model has been extended to describe[18] the preamorphization stages that occur below the stopping power threshold. An analytical treatment was then developed to calculate the cumulative concentration of defects generated via the quenching of the spike. The approach has the advantage of explaining in a conceptually simple way the main trends of experimental results (e.g., the evolution of the crystalline-amorphous boundary with fluence), as well as highlighting the main parameters to be considered. However, there are a few important disadvantages. In particular, the model uses only average defect concentrations as a function of depth in the sample and thus cannot take into account the effect of statistical fluctuations, especially important for low fluences.

In this work we present a Monte Carlo (MC) program that, based on the same formulas applied to the analytical model, may help solve some of these difficulties. For example, one of the advantages of the MC approach is that it accounts for the roughness of the amorphous-crystalline boundary and consequently allows to make predictions about the smoothness in the variation of physical properties (e.g., refractive index) around the boundary. Moreover, it allows to take readily into account the modification of sample density as irradiation proceeds. Finally, the MC simulations can also describe the kinetics of amorphization as a function of fluence before a full homogeneous layer is generated. We explain the algorithm and illustrate its output using as a suitable example the irradiation of a $LiNbO_3$ crystal with a beam

a)Electronic mail: gaston.garcia@uam.es

 © 2006 American Institute of Physics

Downloaded 23 Jan 2013 to 161.111.22.141. Redistribution subject to AIP license or copyright; see http://jap.aip.org/about/rights_and_permissions

of Si ions in the energy range of 5–7.5 MeV. The simulation results are compared to our analytical model and to experimental results obtained at the 5 MV accelerator of the Centre for Microanalysis of Materials (CMAM) (Universidad Autónoma Madrid, Spain), as well as other relevant experimental data.

II. BRIEF DESCRIPTION OF THE PHYSICAL MODEL

The thermal spike model used in this work is as follows. The energy electronically dissipated by the incoming ion with stopping power $S_e(z)$ at depth z generates an excited electron cloud that rapidly transfers the excitation energy to the ionic lattice. Therefore, the temperature rises locally and generates the thermal spike. We assume that the radial temperature profile around the ion trajectory keeps Gaussian during the cooling of the spike and can be written[13] as

$$T(t,r,S_e) = T_s + T_0 e^{-r^2/2a^2(t)},$$

$a(t)$ being the width of the distribution, T_s the substrate temperature, and

$$T_0 = \frac{gS_e}{2\pi a_0^2 \rho C},$$

where S_e is the electronic stopping power, ρ the density, C the specific heat, g an efficiency factor, and $a_0=a(0)$. Local defect concentration $c(r,S_e)$ is assumed to correspond to thermal equilibrium at the maximum temperature $\bar{T}(r,S_e)$ reached during cooling at a distance r from the track axis. The dependence is given by the Arrhenius law that yields

$$c(r,S_e) = Ae^{-\epsilon/k\bar{T}(r,S_e)}, \quad (1)$$

ϵ being the thermal formation energy of the defects, A a constant, and k the Boltzmann constant. The maximum temperature appearing in the formula above is

$$\bar{T}(r,S_e) = T_s + \frac{gS_e}{2\pi a_0^2 \rho C} e^{-r^2/2a_0^2}, \quad 0 < r < \sqrt{2}a_0,$$

$$\bar{T}(r,S_e) = T_s + \frac{gS_e}{\pi e \rho C} \frac{1}{r^2}, \quad r > \sqrt{2}a_0. \quad (2)$$

When $c(r,S_e)$ reaches a critical concentration c_m to cause crystal melting $T=T_m$ (i.e., S_e is equal to a critical value S_m), the lattice becomes locally amorphized after quenching. The effect of successive impacts is cumulative, i.e., the defect concentration at a given point is just the sum of the concentrations attained under each of the single impacts. In particular, for ions and energies above threshold and fluences leading to the overlapping of the individual latent tracks, a homogeneous amorphous layer is generated. Due to the cumulative character of the damage the critical concentration c_m can be reached even for stopping powers below threshold if enough irradiation fluence is given to the sample. Then, on increasing fluence, the critical amorphization condition is reached at progressively deeper levels (this is the situation when the electronic stopping power is monotonically decreasing from the surface inwards), and so the amorphous-crystalline boundary propagates until the ion end of range depth is finally reached.

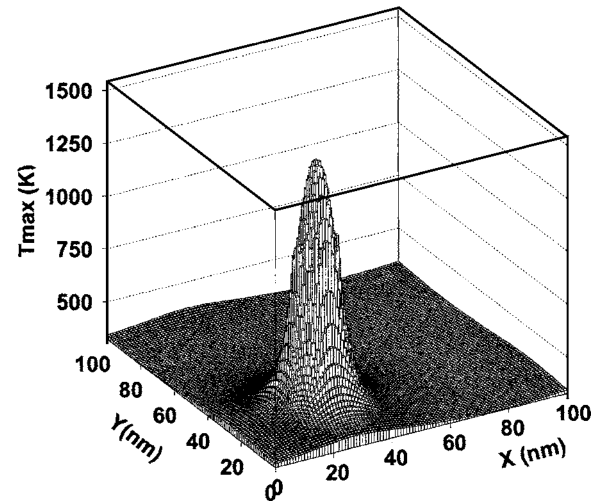

FIG. 1. Maximum teperature map at the XY surface layer of a $LiNbO_3$ sample, generated by a single 7.5 MeV Si ion impact. The model parameters used in the simulation are a_0=5.5 nm, S_m=5.2 keV/nm, and kT_m/ϵ=0.2.

III. DESCRIPTION OF THE MC ALGORITHM

The algorithm proceeds with the following steps:

- The sample is divided into layers parallel to the surface (typically 100 layers), labeled by their depth z.
- For each given layer a 100×100 grid is defined, with pixels of 1 nm^2.
- Each ion impact is generated by choosing random X, Y values in the range $0<X$, $Y<100$. Normal incidence and rectilinear propagation inside the crystal are assumed. Each MC event is thus representing an ion fluence of $1/10^4$ nm^2=10^{10} cm^{-2}.
- A maximum temperature map is generated on the two-dimensional (2D) grid using the formula

$$\bar{T}(r) = T_s + \frac{S_e(T_m - T_s)}{S_m} e^{-r^2/2a_0^2}, \quad r^2 < 2a_0^2,$$

$$\bar{T}(r) = T_s + \frac{2S_e(T_m - T_s)a_0^2}{eS_m r^2}, \quad r^2 > 2a_0^2, \quad (3)$$

which is easily derived from Eq. (2). This is made for each z layer. In each case S_e is obtained from the $S_e(z)$ curve by replacing the z value that corresponds to the z layer considered, whereas r is the distance between the generated impact point and the coordinates of the center of each pixel. Periodic boundary conditions are applied to the temperature map, in such a way that the tails of the profile are recovered at the opposite edge of the grid whenever near-boundary impacts occur (see, as an example, Fig. 1, explained below in the text).

- The temperature maps are translated into defect density ones by usage of

Downloaded 23 Jan 2013 to 161.111.22.141. Redistribution subject to AIP license or copyright; see http://jap.aip.org/about/rights_and_permissions

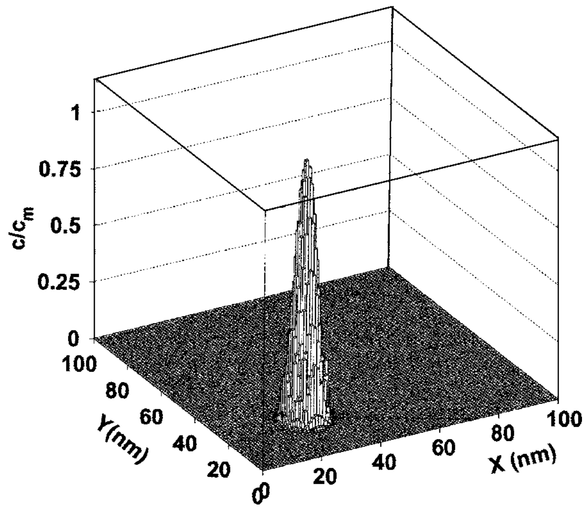

FIG. 2. Normalized defect concentration map at the *XY* surface layer of a $LiNbO_3$ sample, generated by a single 7.5 MeV Si ion impact. The model parameters used in the simulation are a_0=5.5 nm, S_m=5.2 keV/nm, and kT_m/ϵ=0.2.

$$\frac{c}{c_m} = \exp\left(-\frac{T_m/T-1}{kT_m/\epsilon}\right), \tag{4}$$

also easily derived from Eq. (1). Defect concentration is always taken as a quantity normalized to its critical value for amorphization.

- Finally these defect maps generated by the current single event in the loop are added up to cumulative defect concentration maps that have the same structure.
- After updating the damage maps at all z layers for the current ion, the program analyzes the defect concentration data, generating a density correction associated to partial or total amorphization and updating the physical depth of the test layers as well as the stopping power data. This feature of the program is only relevant if the combination fluence/stopping power is strong enough so as to generate amorphous layers somewhere in the sample. The details of this step are explained in the next section.
- When the target fluence is reached the loop is stopped and the accumulated defect concentration maps of the different test layers are retrieved, together with their physical depth values. This is the *raw* output of the simulation program.

IV. SIMULATION RESULTS

A. Basic statistical analysis of damage maps

Figure 1 shows the map of maximum temperatures $\bar{T}$ derived from Eq. (3), for a 7.5 MeV Si ion impact, taken at the surface of a $LiNbO_3$ sample. The defect concentration map corresponding to the same event and derived from Eq. (4) is shown in Fig. 2. The strongly nonlinear Arrhenius law causes a remarkable narrowing of the defect profile in comparison to the temperature one. The effect of successive impacts is illustrated in Figs. 3 and 4. It can be clearly seen that the damage concentration topography across a sample layer is far from being homogeneous, especially for low to moderate ion fluences. Therefore using the average defect concentration (as one is forced to do in our analytical model) can be a rather gross approximation. A first processing stage of the data can be obtained by calculating the normalized areal defect concentration distribution, for each depth layer, i.e., the curve $(1/A)[dA(\bar{c})/d\bar{c}]$ where $\bar{c}=c/c_m$. This function represents the fraction dA of the irradiated area A for which the normalized defect concentration has reached a value lying between $\bar{c}$ and $\bar{c}+d\bar{c}$. Notice that, for example, the integral of this curve above the limit $\bar{c}=1$ corresponds to the fraction of the area which is amorphized at the depth of the corresponding layer.

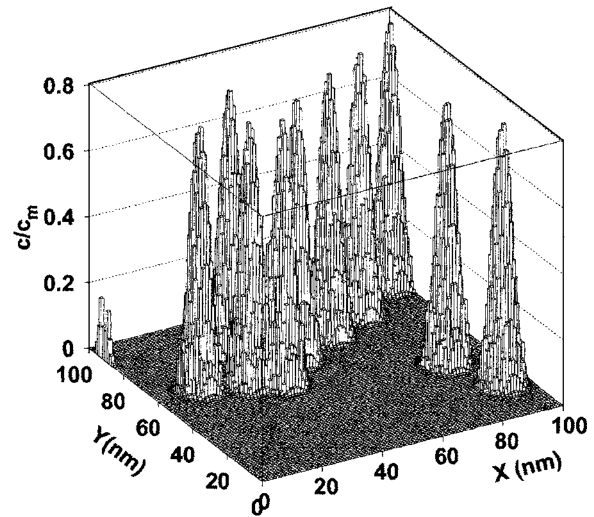

FIG. 3. Defect concentration profile normalized to the critical amorphization value, at the *XY* surface layer of a $LiNbO_3$ sample, generated by 10 ($\Phi = 10^{11}$ cm^{-2}) impacts. Bombarding ions are Si at 7.5 MeV. The model parameters used in the simulation are a_0=5.5 nm, S_m=5.2 keV/nm, and kT_m/ϵ=0.2.

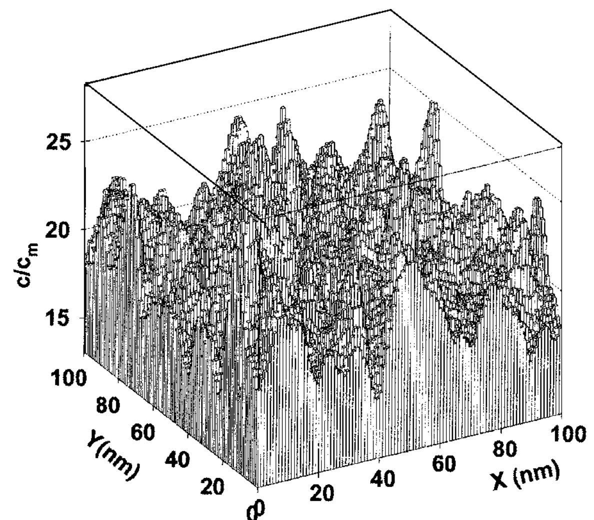

FIG. 4. Defect concentration profile normalized to the critical amorphization value, at the *XY* surface layer of a $LiNbO_3$ sample, generated by 10^4 ($\Phi = 10^{14}$ cm^{-2}) impacts. Bombarding ions are Si at 7.5 MeV. The model parameters used in the simulation are a_0=5.5 nm, S_m=5.2 keV/nm, and kT_m/ϵ=0.2.

Downloaded 23 Jan 2013 to 161.111.22.141. Redistribution subject to AIP license or copyright; see http://jap.aip.org/about/rights_and_permissions

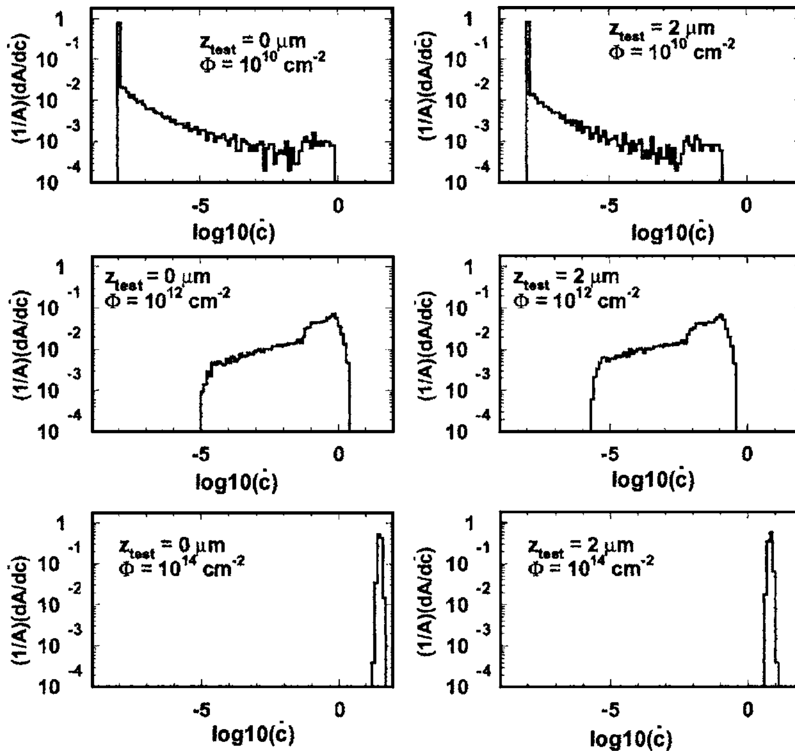

FIG. 5. Normalized areal defect concentration distribution at depths $z_{test}=0$ and 2 μm in a $LiNbO_3$ sample, for 7.5 MeV Si ion fluences $\Phi=10^{10}$, 10^{12}, and 10^{14} cm^{-2}. The model parameters used in the simulation are $a_0=5.5$ nm, $S_m=5.2$ keV/nm, and $kT_m/\epsilon=0.2$.

Figure 5 shows areal defect concentration distributions for two depths and three fluences. It can be observed that most of the area is unaffected by damage at low fluences. Only above 10^{12} cm^{-2} a peak value can be clearly defined for $\bar{c}$. Once this is the case, it becomes resonable to summarize the information contained in the distribution into a single number (namely, the mean or the peak value of $\bar{c}$). A result of this analysis is that neglecting altogether the effect of fluctuations (as it is done in the analytical approach) is not a problem for $\Phi > 10^{12}$ cm^{-2}.

B. Online updating of stopping power

A very direct feedback provided to the MC program, inside the event loop, by simple statistical ellaboration of the raw data (as mentioned in Sec. III) is the online updating of stopping power.

The fraction of the area that has become amorphous at a depth z, hereon denoted as $f_a(z)$, can be derived from the 2D defect concentration map corresponding to the ith depth layer. If this calculation is made inside the event loop of the MC program, the amorphous fraction depth profile $f_a(z)$ can be used to update continuously the depth profiles of any relevant physical property affected by the amorphous/crystalline state of the sample, such as density (and therefore stopping power). A given density change has to be assumed when going from crystal to amorphous. This value has been chosen as 15%, based both on refractive index data and on indications given by previously published results.[11,18] This online updating of stopping power allows to dynamically take into account the total or partial production of amorphous layers, in order to faithfully replicate the actual pattern of ion energy deposition as the simulated irradiation proceeds.

V. COMPARISON OF SIMULATION AND DATA

In this section the MC simulations will be compared to the experimental data obtained for $LiNbO_3$ irradiated with Si at 7.5 and 5 MeV.[10,11] The data give the position of the crystalline-amorphous boundary as a function of fluence. The irradiation experiments were performed at the standard beamline[19,20] of the 5 MV tandem accelerator installed at CMAM at the University Autónoma de Madrid.[20,21] Some additional data on the fraction of amorphized area at the surface have been obtained in this work. The characterization of the damage and amorphization was made by using optical (dark-mode) techniques to measure the refractive index change and Rutherford backscattering spectroscopy (RBS) channeling to determine the occurrence and extension of amorphous regions. The comparison will also include the analytical results reported in a previous paper.[18]

A. Inward propagation of the amorphization boundary with fluence

Using the procedure leading to Fig. 5 one can readily simulate the amorphous fraction f_a produced at a certain depth under given irradiation conditions. Figure 6 shows the amorphous fraction as a function of depth for a sample irradiated with 7.5 MeV Si at several fluences. Full amorphization at the surface is achieved above 10^{13} cm^{-2}. These data can be further analyzed by calculating, for each ion fluence, the depth at which f_a reaches a fixed reference value p (typically $p=0.1$, 0.5, or 0.9). This depth, denoted as z_a^p, can be referred to as *amorphous boundary*. Notice that when $p=0.5$, this boundary separates regions of the crystal in which the amorphous fraction is above or below 50%. When a different p value is used, the meaning of the z_a^p parameter changes consequently.

Downloaded 23 Jan 2013 to 161.111.22.141. Redistribution subject to AIP license or copyright; see http://jap.aip.org/about/rights_and_permissions

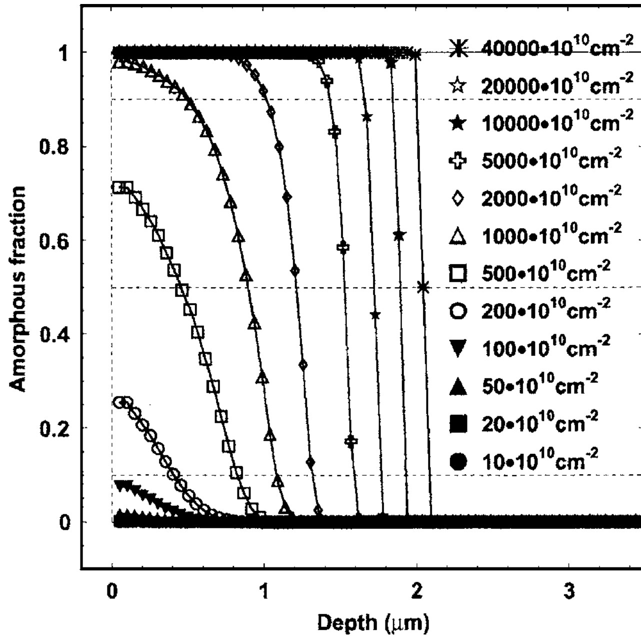

FIG. 6. Amorphized fraction (f_a) as a function of depth in a $LiNbO_3$ sample, for 7.5 MeV Si ion fluences $\Phi=10^{11}-4\times10^{14}$ cm^{-2}. The model parameters used in the simulation are a_0=5.5 nm, S_m=5.2 keV/nm, and kT_m/ϵ=0.2.

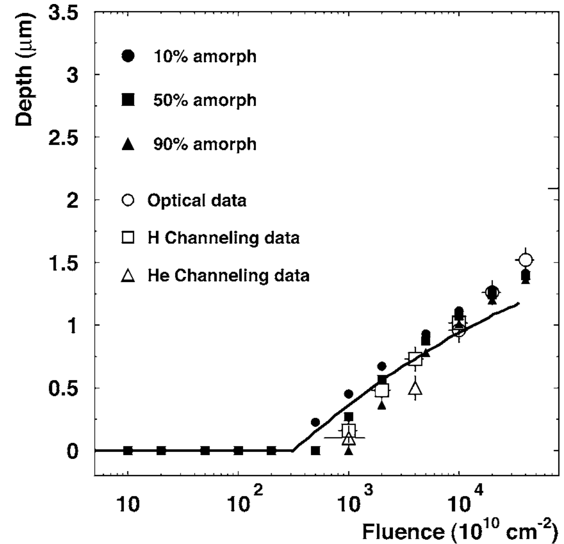

FIG. 8. Simulated amorphous boundary depth as a function of the 5 MeV Si ion fluence, for different p values (full symbols). Analytical model results (full line) and experimental data (open symbols) are shown for comparison. The model parameters used in the simulation are a_0=5.5 nm, S_m =5.2 keV/nm, and kT_m/ϵ=0.2.

Figures 7 and 8 show the position of the amorphous-crystalline boundary z_a^p as a function of fluence (irradiation with 7.5 and 5 MeV Si beam) for a few p values, as compared to the result of the analytical model (the model presented in Ref. 18 is updated by the implementation of an accurate substrate temperature correction, which changes slightly the results) proposed in Ref. 18 and to experimental optical and RBS-channeling data.[11] The agreement between experiment and simulation is quite reasonable for the two beam energies. Notice that, as expected, the p value used to define the amorphous boundary becomes more and more irrelevant as fluence increases. For low fluences, however, it is essential to choose properly the p value that can be compared to the experimental data available. For example, if the amorphous boundary is measured by refractive index sensitive techniques (like in Ref. 11), it is most reasonable to use p =0.5. In the case that RBS-channeling data are available, different p values can, in principle, be used by correctly analyzing the experimental spectra.

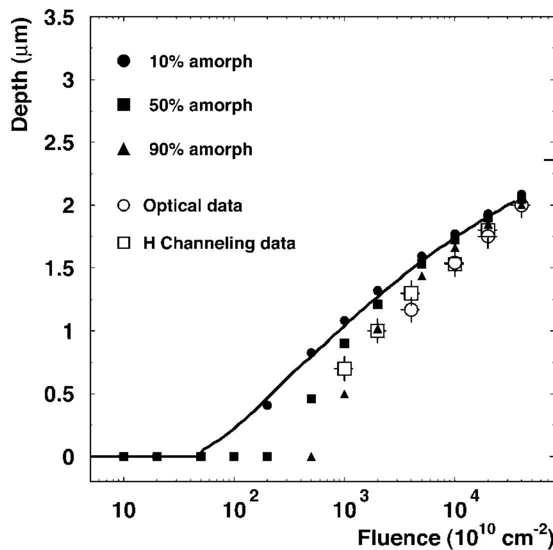

FIG. 7. Simulated amorphous boundary depth as a function of the 7.5 MeV Si ion fluence, for different p values (full symbols). Analytical model results (full line) and experimental data (open symbols) are shown for comparison. The model parameters used in the simulation are a_0=5.5 nm, S_m =5.2 keV/nm, and kT_m/ϵ=0.2.

B. Amorphous fraction at the sample surface

Figures 9 and 10 show the amorphous fraction f_a at the

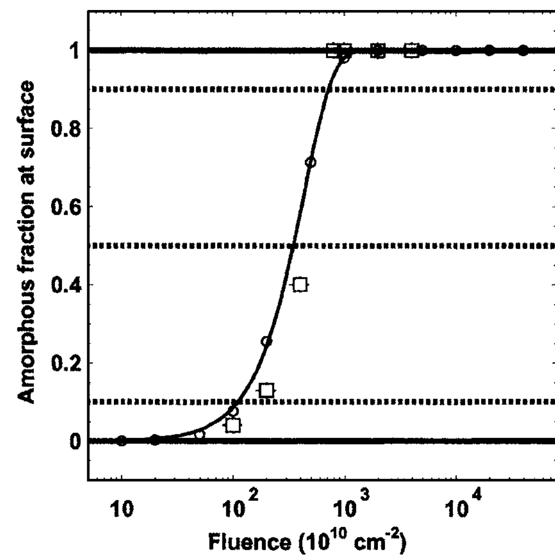

FIG. 9. Simulated amorphous fraction (f_a) as a function of the 7.5 MeV Si ion fluence, at the sample surface (open circles). The model parameters used in the simulation are a_0=5.5 nm, S_m=5.2 keV/nm, and kT_m/ϵ=0.2. The curve shows the result of fitting an Avrami curve to the MC results (full line), the result of the fit being a=4.78±0.17 nm and n=1.6±0.2. Channeling data obtained with a H (open squares) beam are shown for comparison.

Downloaded 23 Jan 2013 to 161.111.22.141. Redistribution subject to AIP license or copyright; see http://jap.aip.org/about/rights_and_permissions

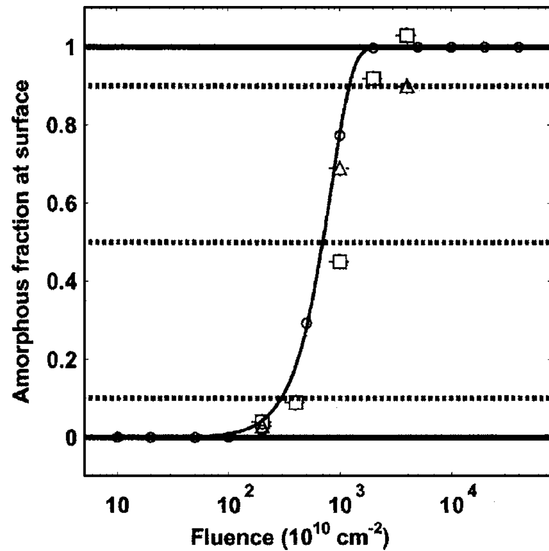

FIG. 10. Simulated amorphous fraction (f_a) as a function of the 5 MeV Si ion fluence, at the sample surface (open circles). The model parameters used in the simulation are a_0=5.5 nm, S_m=5.2 keV/nm, and kT_m/ϵ=0.2. The curve shows the result of fitting an Avrami curve to the MC results (full line), the result of the fit being a=3.47±0.10 nm and n=2.2±0.3. Channeling data obtained with a H (open squares) and He (open triangles) beam are shown for comparison.

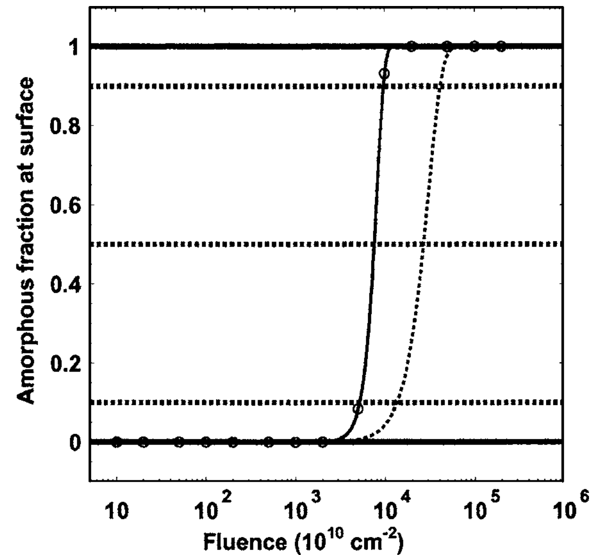

FIG. 11. Simulated amorphous fraction (f_a) as a function of the O (5 MeV) ion fluence, at the sample surface (open circles). The model parameters used in the simulation are a_0=5.5 nm, S_m=5.2 keV/nm, and kT_m/ϵ=0.2. The curve shows the result of fitting an Avrami curve to the MC results (full line), the result of the fit being a_{MC}=1.11±0.03 nm and n_{MC}=4.9±1.0. The Avrami result from Ref. 9 is also shown (dotted line) for comparison, the value of the parameters being a=0.57±0.06 nm and n=2.75±0.25.

sample surface as a function of the ion fluence. The simulation corresponds to irradiations with 7.5 (Fig. 9) and 5 (Fig. 10) MeV Si. The experimental amorphous fraction was determined through the expression $f_a=[Y_{ch}(\Phi)-Y_{ch}(0)]/[Y_r-Y_{ch}(0)]$ where Y_r and $Y_{ch}(\Phi)$ are, respectively, the RBS yields corresponding to random and channeled incidence (in the latter case, after irradiation with a fluence Φ). The MC results have been successfully fitted by using an Avrami curve,

$$f_a = 1 - \exp[-(a^2\phi)^n].$$

Notice that this expression includes two free parameters. The first one, a has distance dimensions, the result of the fit being a=4.78±0.17 nm (7.5 MeV Si) and a=3.47±0.10 nm (5 MeV Si). Clearly a gives an estimate of the dimensions of the region affected by each single impact. The second free parameter is the exponent n, which accounts for the degree of the nonlinearity of the accumulation process, n=1 being the limit that reduces the problem to pure Poisson statistics (i.e., a static amorphization threshold not depending on prior fluence). The result of the fit is n=1.6±0.2 (7.5 MeV Si) and n=2.2±0.3 (5 MeV Si). The simulation shows good agreement with the experimental data obtained by H and He channeling analyses.

Prior experimental data on this topic have been reported[9] for $LiNbO_3$ irradiated with O at 5 MeV. The data were fit with an Avrami law having a=0.57±0.06 nm and n=2.75±0.25. As shown in Fig. 11, we have tried our MC simulations (open symbols) to account for the Avrami fit of the data (dotted line). The curve derived from the MC results, included as a solid line, yields a_{MC}=1.11±0.03 nm and n_{MC}=4.9±1.0. The errors quoted only account for statistical fluctuations. Notice that the value of a changes markedly with respect to the silicon cases, reflecting the strongly nonlinear dependence of the critical fluence for full layer amorphization with the electronic stopping power. Specifically in the case of the oxygen data, in spite of the disagreement in the fluence at which the effect takes place, the simulation markedly agrees with the Avrami-like behavior of the data. It is remarkable that the Avrami dependence predicted by our model emerges from a simple law of damage accumulation, without the need of invoking specific mechanisms of defect nucleation.

VI. CONCLUSIONS

In this paper a MC algorithm is used to implement a previous model based on thermal generation of defects under ion beam irradiation. It is a flexible tool that provides a deeper understanding about ion induced amorphization phenomena in crystalline samples. The main advantages of this MC approach are the following: (a) it takes into account statistical fluctuations; (b) the irradiation can be "replayed"; and (c) it could be easily extended to include defects created by an additional mechanism such as nuclear collisions.

It is planned to use this tool routinely to understand the results of experiments being carried out at the 5 MV accelerator of CMAM (Universidad Autónoma Madrid, Spain).

[1] J. K. Hirvonen, *Ion Implantation and Ion Beam Processing* (North-Holland, Amsterdam, 1984).
[2] F. Agulló-López, C. R. A. Catlow, and P. D. Townsend, *Point Defects in Materials* (Academic, London, 1988).
[3] J. P. Ziegler, *Ion Implantation Technology* (North-Holland, Amsterdam, 1992).
[4] P. D. Townsend, P. J. Chandler, and L. Zhang, *Optical Effects of Ion Implantation* (Cambridge University Press, Cambridge, 1994).
[5] K. Bethge and R. Spohr, in *Ion Tracks and Microtechnology: Basic Principles and Applications* (Vieweg, Braunschweig, 1990).
[6] M. Toulemonde, S. Bouffard, and F. Studer, Nucl. Instrum. Methods Phys. Res. B **91**, 108 (1994).

Downloaded 23 Jan 2013 to 161.111.22.141. Redistribution subject to AIP license or copyright; see http://jap.aip.org/about/rights_and_permissions

[7]M. Toulemonde, C. Trautmann, E. Balanzat, K. Hjort, and A. Weidinger, Nucl. Instrum. Methods Phys. Res. B **216**, 1 (2004).
[8]G. G. Bentini *et al.*, J. Appl. Phys. **92**, 6477 (2002).
[9]G. G. Bentini *et al.*, J. Appl. Phys. **96**, 242 (2004).
[10]J. Olivares, G. García, F. Agulló-López, F. Agulló-Rueda, J. C. Soares, and A. Kling, Nucl. Instrum. Methods Phys. Res. B **242**, 534 (2005).
[11]J. Olivares, G. García, F. Agulló-López, F. Agulló-Rueda, A. Kling, and J. C. Soares, Appl. Phys. A: Mater. Sci. Process. **81**, 1465 (2005).
[12]J. Olivares, G. García, A. García-Navarro, F. Agulló-López, O. Caballero, and A. García-Cabañes, Appl. Phys. Lett. **86**, 183501 (2005).
[13]G. Szenes, Phys. Rev. B **51**, 8026 (1995).
[14]B. Canut and S. M. M. Ramos, Radiat. Eff. Defects Solids **145**, 1 (1998).
[15]M. Toulemonde, Ch. Dufour, A. Meftah, and E. Paumier, Nucl. Instrum. Methods Phys. Res. B **166–167**, 903 (2000).
[16]E. M. Bringa, R. E. Johnson, and M. Jakas, Phys. Rev. B **60**, 15107 (1999).
[17]M. Jakas, E. M. Bringa, and R. E. Johnson, Phys. Rev. B **65**, 165425-1 (2002).
[18]F. Agulló-López, G. García, and J. Olivares, J. Appl. Phys. **97**, 093514 (2005).
[19]A. Climent-Font, F. Paszti, G. García, M. T. Fernández-Jiménez, and F. Agulló-López, Nucl. Instrum. Methods Phys. Res. B **219–220**, 400 (2004).
[20]www.uam.es/cmam
[21]D. J. W. Mous, A. Gottdang, R. G. Haitsma, G. García López, A. Climent-Font, F. Agulló-López, and D. O. Boerma, AIP Conf. Proc. **680**, 999 (2003).

Downloaded 23 Jan 2013 to 161.111.22.141. Redistribution subject to AIP license or copyright; see http://jap.aip.org/about/rights_and_permissions